Autosegmentation of the Attachment Sites of the ACL Utilizing Two Planes of MR Imaging

Jefferson R. Bercaw[1], Jay P. Willhite[2], Olivia C. O'Reilly[2], Robert T. Tisherman[2], Meghan Gill[1], Roarke W. Horstmeyer[1], Jocelyn R. Wittstein[2], Charles E. Spritzer[2], Louis E. DeFrate[1,2]
[1]Duke University, Durham, NC; [2]Duke University School of Medicine, Durham, NC
jrb187@duke.edu

Disclosures: JRB (N), JPW (N), OCO (6-Arthrex, Smith & Nephew, Stryker, Zimmer Biomet, Depuy Synthes, Verticel), RTT (3B-Arthrex), MG (3A-Synchron), RWH (4-Ramona Optics Inc.), JRW (N), CES (1-UpToDate), LED (8-*Am J Sports Med, J Orthop Res, J Biomech*)

INTRODUCTION: ACL injuries affect hundreds of thousands of individuals each year, and can lead to significant acute and chronic negative outcomes [1]. In order to study the biomechanics of the ACL, as well as to ensure anatomic graft placement during ACL reconstruction, many studies have focused on identifying the ACL's attachment sites [2, 3]. Previously, our lab has developed and validated a method for segmenting the ACL attachment sites from multiple planes of knee magnetic resonance (MR) imaging [4, 5]. However, manual segmentation requires extensive training, and is time intensive. Convolutional neural networks (CNNs) have automated other MR segmentation tasks, and may serve as a fast and reliable means to segment the attachment sites of the ACL. Therefore, the goals of this study were (1) to develop machine learning (ML) networks to segment the attachment sites of the ACL from knee MR scans, and (2) to evaluate the ability of these networks to identify the length of the ACL at the time of MR acquisition. We hypothesized that ML methods using two planes of imaging will outperform those using only one plane, and that automated segmentation will reliably measure ACL length.

METHODS: Dataset: This study used MR knee scans taken from 51 participants with no history of lower limb injury or surgery from IRB-approved studies (26 males, 25 females; mean (range) age: 26 (19-35 years); BMI: 23.8 (18.1 – 32.0 kg/m^2)). For each participant, sagittal, axial, and coronal double-echo steady-state (DESS) images (FA: 25°, TR: 17ms; TE: 6ms; resolution: 0.3x0.3x1.0 mm) were acquired on a 3.0 T MR scanner with an 8- or 15-channel knee coil (Trio Tim, Siemens; Prisma, Siemens). An experienced segmenter was trained by two musculoskeletal radiologists and labeled the tibial ACL attachments on sagittal and coronal images, and the femoral ACL attachments on axial and coronal images. Image Pre-Processing: Image volumes were linearly interpolated in the slice direction to create cubic voxels. Sagittal and axial image volumes were registered to the coronal image volumes via affine transformations calculated from surface registration (MATLAB R2023b) of the tibiae and femora, respectively. This process resulted in spatial correspondence between voxels across image volumes. Each pair of image volumes (tibia: sagittal and coronal; femur: axial and coronal) was cropped to 128x128x128 voxels. Label Pre-Processing: The sagittal (tibial attachment) and axial (femoral attachment) segmentations were transformed into the coronal representation, and converted into point clouds (**Figure 1A**). Surfaces of the attachments were created (Geomagic Wrap 2024), and converted to a binary label mask. Dataset Preparation: A 3-fold cross-validation strategy was employed, where, in each fold, an 80% training, 10% testing, and 10% validation data split was performed with unique testing and validation participants across folds. Training datasets were augmented, where each image volume and label were duplicated 5 times and randomly translated. Model Training and Evaluation: Three architectures were tested: a 2D Attention U-Net utilizing one plane of imaging, a double 2D Attention U-Net- utilizing both planes of imaging, and a 3D Attention U-Net utilizing both planes of imaging [6]. Hyperparameters were optimized with a grid search technique. The Tversky loss function [7] and ADAM optimizer [8] were used. The mean dice similarity coefficient (DSC) in the testing datasets across all folds were used to evaluate performance. Models with the highest mean DSCs were used for model application. Model Application: The predicted and manual surfaces for both attachment sites for each participant were used to calculate the ACL length (distance between tibial and femoral attachment site centroids) at the time of MR acquisition. Predicted and manual lengths of the ACL were compared via their mean difference and a two-way mixed effects intra-class correlation coefficient (ICC) for absolute agreement (R 4.4.1).

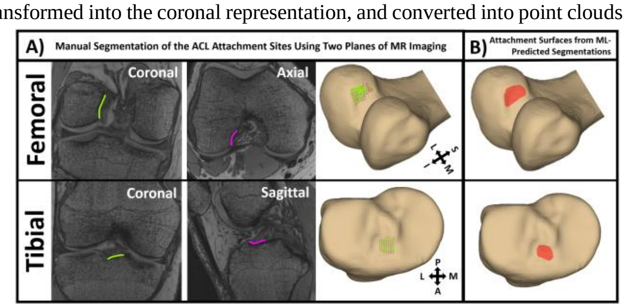

Figure 1*: Manual and predicted attachment sites of the ACL for a subject in the testing dataset. The attachment sites were manually segmented from two planes of MRI (****A****). The 3D Attention U-Net uses both image volumes to predict voxels, which were used to create attachment surfaces (****B****).*

Attachment	Input View(s)	Architecture	DSC Mean (SD)
Tibial	Coronal	2D	0.493 (0.112)
	Sagittal	2D	0.490 (0.087)
	Coronal + Sagittal	Double 2D	0.518 (0.085)
	Coronal + Sagittal	**3D**	**0.592 (0.103)**
Femoral	Coronal	2D	0.522 (0.085)
	Axial	2D	0.498 (0.097)
	Coronal + Axial	Double 2D	0.579 (0.090)
	Coronal + Axial	**3D**	**0.594 (0.104)**

Table 1*: Testing dataset model comparisons.*

RESULTS: The 3D Attention U-Nets yielded the highest testing dataset mean DSCs for both attachment sites (**Table 1**). The mean difference in ACL length as measured manually and automatically was 0.12 mm, representing 0.4% of its length. Predicted and manual ACL lengths demonstrated good reliability (ICC = 0.863).

DISCUSSION: This study developed ML networks to segment the attachment sites of the ACL from two planes of MR imaging, and evaluated their ability to measure the length of the ACL. First, this study found that 3D architectures outperformed 2D architectures for this task. Additionally, this study found that a dual-plane approach may be more beneficial than a single-plane approach when segmenting the ACL attachment sites with ML techniques (**Figure 1B**). As the ACL runs obliquely to all three imaging planes, image volumes captured from different directions may provide additional information that improves the segmentation of the attachment sites. Overall, DSCs reported herein were lower compared to other knee MR segmentation tasks, such as bone or cartilage [9] (DSCs > 0.9). Differences in DSCs across these tasks are likely due to class imbalance within this dataset, as the ACL attachment sites had a very limited volume in the image. To address this challenge, the Attention U-Net and Tversky loss were employed, as they have been previously shown to improve model performance in other class imbalanced segmentation tasks [10]. Importantly, anatomic graft placement may provide the best opportunity to restore native knee biomechanics [11] and reduce risk of osteoarthritis [12], and these ML tools could serve as an automatic and patient-specific method to improve pre-surgical planning via imaging of the uninjured limb. Lastly, the centroid-to-centroid length of the ACL at the time of MR acquisition as measured manually and automatically demonstrated good reliability (**Figure 2**; mean difference = 0.12 mm; ICC = 0.863). This study supports the use of these techniques when studying the ACL. A limitation of this work was its young and healthy cohort. The performance of these networks on older participants, or on those with ACL injury is unknown. Nonetheless, this study developed ML models that automatically segmented the ACL attachment sites in vivo, and reliably measured ACL length.

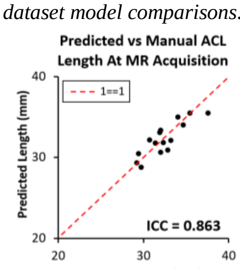

Figure 2*: Manual and predicted ACL lengths for all subjects (n = 15) within the testing datasets.*

SIGNIFICANCE/CLINICAL RELEVANCE: This study developed ML networks that automatically segmented the attachment sites of the ACL, and reliably measured ACL length. As ACL injuries affect hundreds of thousands each year, these tools will aid in the study of ACL biomechanics, and may also provide a framework for achieving anatomic ACL graft placement.

REFERENCES: [1] Sanders et al., *Am J Sports Med*, 2016; [2] Foody et al., *Am J Sports Med*, 2023; [3] Markatos et al., *Eur J Orthop Surg Traumatol*, 2012. [4] Abebe et al., *Am J Sports Med*, 2009; [5] Taylor et al., *J Biomech*, 2013; [6] Oktay et al., *CVPR*, 2018; [7] Salehi et al., *CVPR*, 2017; [8] Kinga and Ba, *ICLR*, 2015; [9] Bradley et al., *Osteoarthr Cartil Open*, 2025; [10] Abraham and Khan, *ISBI*, 2019; [11] DeFrate, *J Orthop Res*, 2017; [12] Cinque et al., *Am J Sports Med*, 2022.

ACKNOWLEDGEMENTS: We acknowledge our funding sources for this project, including the National Institute of Health. We also acknowledge the Duke University Center for Magnetic Resonance Development for technical support.